Noninvasive Visualization and Analysis of Parafoveal Capillaries in Humans

Johnny Tam,[1] *Joy A. Martin,*[2] *and Austin Roorda*[1,3]

PURPOSE. To demonstrate a noninvasive method to visualize and analyze the parafoveal capillary network in humans.

METHODS. An adaptive optics scanning laser ophthalmoscope was used to acquire high resolution retinal videos on human subjects. Video processing tools that enhance motion contrast were developed and applied to the videos to generate montages of parafoveal retinal capillaries. The capillary network and foveal avascular zone (FAZ) were extracted using video and image analysis algorithms. The capillary densities in the zone immediately outside the FAZ were calculated and the variation in density as a function of direction was investigated. Extracted FAZ geometries were used to calculate area and effective diameters. The authors also compared their method against fluorescein angiography (FA) for one subject.

RESULTS. The parafoveal capillaries were clearly visible when the motion contrast in noninvasive videos was enhanced. There was a marked improvement in the contrast of the parafoveal capillaries when compared to the unprocessed videos. The average FAZ area was 0.323 mm^2, with an average effective diameter of 633 μm. There was no variation in capillary density near the FAZ in different directions.

CONCLUSIONS. Using motion cues to enhance vessel contrast is a powerful tool for visualizing the capillary network, in the absence of contrast agents. The authors demonstrate a tool to study the microcirculation of healthy subjects noninvasively. (*Invest Ophthalmol Vis Sci.* 2010;51:1691–1698) DOI:10.1167/iovs.09-4483

The retina is one of the most metabolically active tissues in the human body, and as such, is coupled with a unique system of blood vessels. The inner retinal microvasculature has been mapped out in high resolution using excised monkey retinas.[1] Far from the fovea, the capillary network is multi-layered; closer to the fovea, the network thins down to two layers in the peri- to parafoveal region, and to one layer in the immediate parafoveal region. Finally, in the fovea, there are no vessels, forming the foveal avascular zone (FAZ). The average diameter of a normal FAZ as described in textbooks is around 400 to 500 μm. However, there is considerable individual variation.[2] The FAZ has been well characterized and is of important clinical significance in a number of different diseases, including diabetes.[3]

There are two key challenges that must be addressed when performing optical imaging of the retinal microcirculation: low capillary contrast and aberrations in the eye. Contrast is typically improved using a contrast agent, such as in fluorescein angiography (FA). Although FA is considered to be a "gold standard" for studying retinal vessels, it does carry a small risk for adverse reactions.[4] Due to these risks, FA is not performed on normal eyes, except under special circumstances. Moreover, FA may not be able to reliably identify the smallest capillaries.[5] An alternate method to improve capillary contrast is to use video processing tools based on flow visualization.[6] These tools included mean, variance, min, max, range, and transition images. The variance image has been previously applied as a method for increasing vessel contrast in microvessels before applying leukocyte tracking algorithms.[7] However, the variance image alone fails to increase the contrast of vessels in our datasets. We will demonstrate that spatial and temporal information can be used to increase the local contrast for moving objects, and enable the visualization of capillaries.

Aberrations in the eye, which may hinder the resolution of the smallest capillaries (i.e., those with diameter ~5 μm), can be corrected using adaptive optics.[8] Recently, an adaptive optics scanning laser ophthalmoscope (AOSLO) was used to quantify leukocyte speeds through parafoveal capillaries.[9,10] In this article, we will combine video and image processing tools with AOSLO imaging to demonstrate an improved method that can detect even the smallest capillaries in the parafoveal region without the use of injected dyes.

METHODS

Image Acquisition

All procedures performed in this study adhered to the tenets of the Declaration of Helsinki. After a detailed explanation of the procedures, written informed consent was obtained from all participants. The research protocol was approved by the University of California, Berkeley Institutional Review Board. Videos were acquired on human subjects as described previously,[10] using a variety of imaging parameters. Briefly, videos were acquired at 512 × 512 pixels^2, 30 or 60 fps, for 5 to 40 seconds in overlapping windows in the parafoveal region. The field of view ranged from 1.2° to 2.5°. The imaging wavelength was either 532 nm or 840 nm. (See Figs. 3, 9, and 10 for examples of videos and results using the 532 nm laser, and Figs. 1, 5, 6, and 10 for examples of videos and results using the 840 nm laser.)

Ten subjects with clear ocular media and no history of prior ocular or systemic disease were used. For each subject, a total of 20 to 78 videos were collected. The average age of the subjects was 27 years with a SD of 6.4 years.

Video Processing

Preprocessing. Raw videos were corrected for scanning distortions and stabilized to correct for eye motion, as described pre-
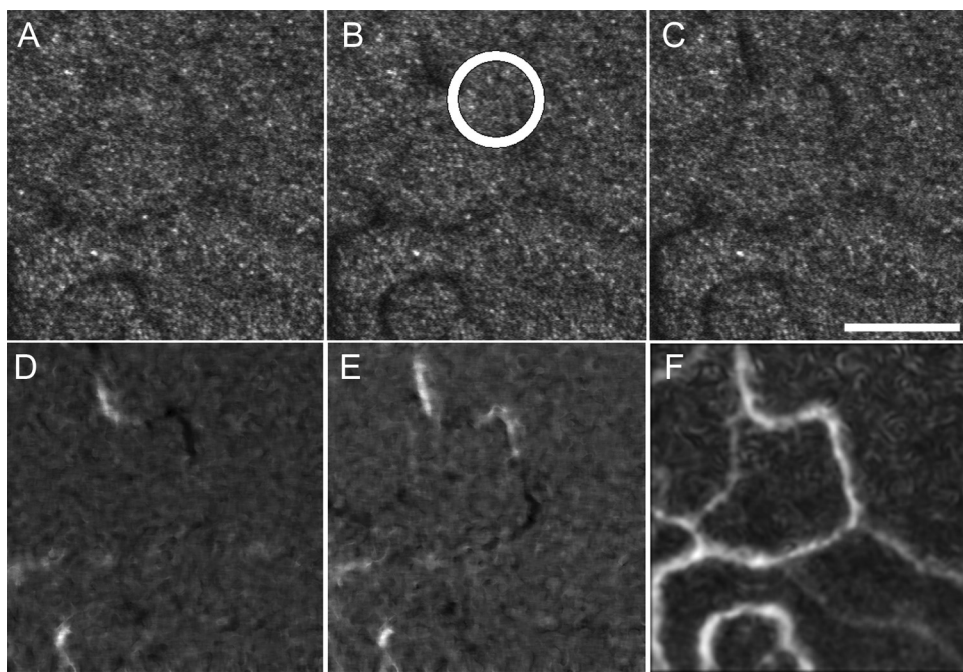
FIGURE 1. High resolution images of the human retina, acquired noninvasively using an 840 nm laser. The video and image processing steps are illustrated. (**A**, **B**, **C**) Three consecutive frames from an unprocessed video. Individual photoreceptors can be seen as small *dots*. However, it is difficult to distinguish the locations of vessels and of individual leukocytes (one leukocyte is shown inside the circle). Scale bar, 100 μm. (**D**) The first step in motion contrast enhancement is the division image, $D_j(x, y)$; (**E**) An averaged division image, $M_j(x, y)$; (**F**) The *highlighted* image, $S(x, y)$, showing perfused vessels.

viously.[11,12] Next, the videos were cropped to eliminate boundary effects due to the eye motion correction, and passed through a median filter to eliminate uneven noise artifacts due to noise redistribution from the desinusoiding step. Finally, when necessary, frames where either the Signal to Noise Ratio (SNR) dropped (e.g., due to high frequency tear film–induced aberrations), or where stabilization failed (e.g., blinks and saccades) were deleted.

Motion Contrast Enhancement. An example of images from an unprocessed video shows that vessel contrast disappears in the presence of leukocytes (Fig. 1). The intensity variations of pixels in vessel regions are similar in magnitude to intensity variations of pixels near photoreceptor boundaries. Our strategy is first, to enhance the contrast of individual fluid parcels, and second, to apply flow visualization tools to the locally enhanced videos.

It is possible to see individual flow parcels traveling through capillaries (Fig. 1). To identify these flow parcels, an approach similar to the difference video technique can be applied. We use multi-frame division videos. Division videos are similar in concept to the difference video, except that instead of subtracting, individual pixels are divided by each other. A division image $D(x, y)$ is calculated from each pair of consecutive frames as $D_j(x, y) = I_j(x, y)/I_{j+1}(x, y)$, where $I_j(x, y)$ represents the intensities of frame j. Consecutive division images are averaged together to create a multi-frame division image, $M_j(x, y) = [D_j(x, y) + D_{j+1}(x, y)]/2$, with high contrast ratios between the fluid

parcels and the background tissue. M_j gives the jth frame of the multi-frame division video.

Finally, the capillaries are visualized by collapsing the multi-frame division video down to a single image (which we call the "highlighted image"). This is done by calculating the SD image of the multi-frame division video. The SD image $S(x, y)$ can be calculated using either arithmetic or geometric definitions. The arithmetic definitions are given by:

$$S(x, y) = \sqrt{\frac{1}{N-1} \sum_{j=1}^{N} [M_j(x, y) - \overline{M}(x, y)]^2}; \quad \overline{M}(x, y) = \frac{1}{N} \sum_{j=1}^{N} M_j(x, y) \quad (1)$$

The geometric definitions are given by

$$S(x, y) = \exp\left(\sqrt{\frac{\sum_{j=1}^{N} [\ln M_j(x, y) - \ln \overline{M}(x, y)]^2}{n-1}} \right); \quad (2)$$

$$\overline{M}(x, y) = \sqrt[n]{\prod_{j=1}^{N} M_j(x, y)}$$
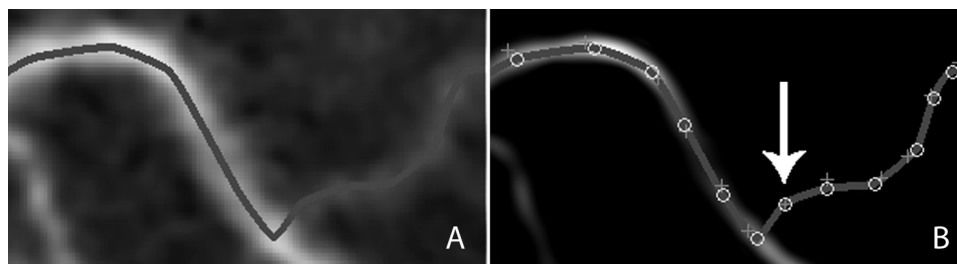
FIGURE 2. Vessels were extracted using a semi-automated procedure. (**A**) A piece of a *highlighted* image at the edge of the FAZ, showing a faint vessel segment connected to a bright vessel segment, with the extracted vessel overlaid as a *thick gray line*. (**B**) The Frangi vesselness measure is used to guide the vessel extraction, with seed points, $p_i(x, y)$, depicted as crosses, and displaced points, $q_i(x, y)$, depicted as *circles*. In areas where there is no information from the vesselness measure (*arrow*), no correction is applied.
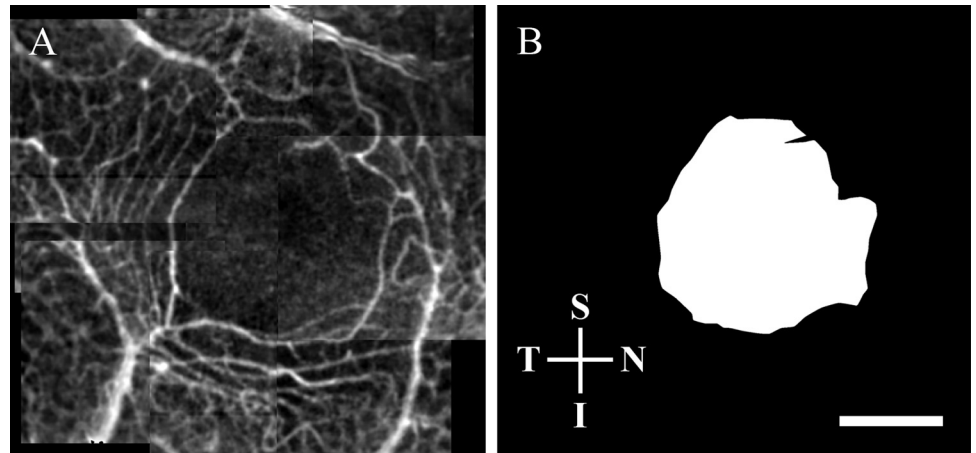
FIGURE 3. An example of FAZ extraction from 532 nm videos. (**A**) Nine overlapping videos were separately processed and then compiled into a montage, showing parafoveal capillaries. (**B**) The FAZ was extracted and used for area quantification. Superior, Inferior, Nasal, and Temporal directions are labeled (S, I, N, T). Scale bar, 300 μm.

We used both arithmetic and geometric definitions. The arithmetic definitions were more robust against noise as well as errors in stabilization, and could be used for general cases, while the geometric definitions gave higher quality results, but required excellent stabilization.

FAZ Quantification

Overlapping videos of the parafoveal region were used to generate a montage. To create montages, each video was analyzed separately, and then maps of highlighted images were pieced together (Adobe Photoshop; Adobe Systems, Inc., San Jose, CA). Auto leveling was used to minimize differences in histogram scaling between videos. The highlighted images were also used to generate a montage of the unprocessed video by registering each highlighted image to its unprocessed image.

We applied custom image analysis tools to the montage of highlighted images to analyze the FAZ. The FAZ boundary was defined as the centerline of the bordering vessels. To extract vessel centerlines, we used a semi-automated method based on the Frangi vesselness measure[13] (Fig. 2), in the following manner. A closed contour $C(t)$ was used to mathematically represent the FAZ boundary. First, through a graphical user interface, seed points $p_i(x, y)$ were selected by the user at points near the boundary of the FAZ. Next, $p_i(x, y)$ were displaced toward the centerline of the nearest vessel to reduce variations due to user input. To identify vessel centerlines, we calculated the Frangi vesselness measure.[13] A neighborhood N_i was generated around each $p_i(x, y)$. The vesselness values in N_i, denoted as V_i, were used to determine the location of the new point, $q_i(x, y)$, as $q_i(x, y) = \max(V_i)$. The amount of displacement from the seed point toward the centerline point was restricted by the size of the neighborhood around which to search. Finally, $C(t)$ was generated using piecewise Cardinal splines

between neighboring pairs of $q_i(x, y)$, with the restriction that interpolation points needed to fall into the pixel space of the montage image. $C(t)$ was used to generate a mask of the FAZ for the area calculation (Fig. 3).

Area was calculated from the mask of the FAZ in pixels^2 and then converted to mm^2 using a model eye parameterized by axial length, anterior chamber depth (ACD), and corneal curvature (CC). Axial length was measured on all subjects. We used ACD and CC values from Bennett's model eye,[14] except in the case of four subjects, where we were able to measure ACD and CC directly (IOL Master; Carl Zeiss Meditec AG, Jena, Germany). The use of additional biometry measurements, such as ACD and CC, improves the conversion from angle to distance; however, the amount of improvement is small.[15] Using ray tracing, the posterior nodal point (PNP) of the eye was estimated from these parameters. Finally, we calculated mm/deg = d*tan(1 deg), where d is the distance from the PNP to the retina.

The effective diameter, d_{eff}, was calculated as the diameter of a circle with equal area

$$d_{\text{eff}} = 2\sqrt{\frac{\text{Area}}{\pi}} \qquad (3)$$

Capillary Density Measurements

Vessels were mapped out and extracted with the same approach used in the FAZ analysis (Fig. 2). Since the microvessels are similarly-sized near the FAZ, we defined capillary density as L_{Tot}/A, where L_{Tot} was the combined length of all capillary segments in a region of interest (ROI), and A the area of the ROI, as described previously.[16] We selected a special ROI to represent the zone at which there was only a single layer of capillaries, with no major retinal vessels (arteries and
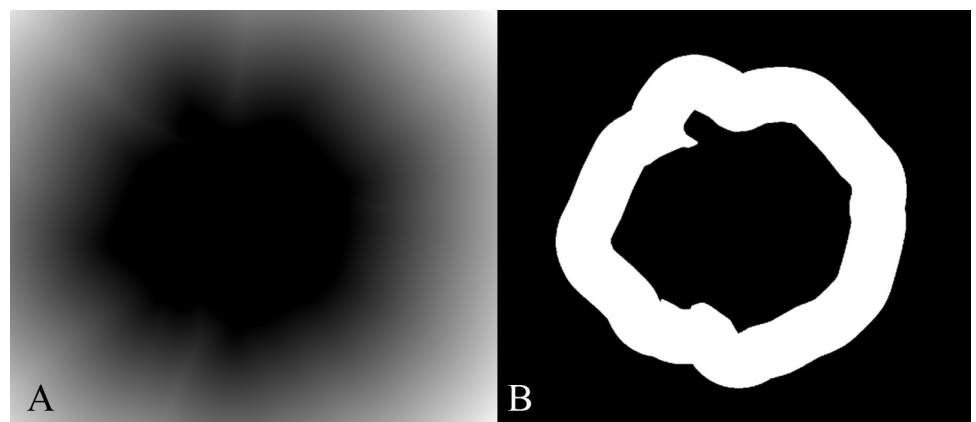
FIGURE 4. Illustration of the automated algorithm for ROI extraction. (**A**) Visual representation of the distance map, showing the distance to the nearest point in the FAZ. Inside the FAZ, the distance is 0 (*black*); as one moves farther away from the FAZ, the distance increases toward the maximum distance (*white*). (**B**) The resulting ROI.
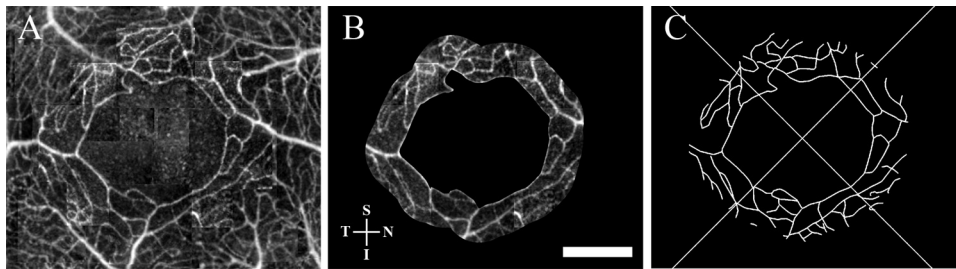
FIGURE 5. Capillary extraction in the ROI, from 840 nm videos. (A) Montage of processed frames showing parafoveal capillaries. (B) Portion of the processed montage corresponding to the ROI. S, I, N, and T directions are labeled. Scale bar, 300 μm. (C) Extracted capillaries, divided into four quadrants originating from the centroid of the FAZ.

veins). In our datasets, this was the zone that was 0.15° from the edge of the irregularly-shaped FAZ.

The ROI was generated automatically from $C(t)$ (Fig. 4) in the following manner. The distance transform[17] was used to calculate the distance of all pixels outside of the FAZ, as defined by $C(t)$. We discarded all pixels that were outside of 0.15° from the edge of the FAZ, as well as pixels that were in the interior of $C(t)$.

To investigate whether there was a variation in capillary density in different directions (e.g., superior versus inferior), we divided the ROI into four quadrants (Fig. 5). These were defined by calculating equiangular line segments radiating outwards from the centroid of the FAZ. We used quadrants to maximize the amount of data used to calculate capillary density, and minimize effects due to the proximity to feeding arterioles, since there is a capillary free zone[18] that surrounds arterioles, which would alter measurements of capillary density. To generate the L_{Tot}/A measure, we took the sum of capillary lengths in each of the quadrants and divided by the area of the ROI contained within the quadrant. To determine statistically whether there was a difference in capillary density in different directions, we used the Kruskal-Wallis one-way ANOVA.[19]

Comparisons

First, since FAs are considered the gold standard for studying the retinal vessels, we performed a comparison between the vessels identified using our method and using a standard FA, for one normal subject. Although FAs are not performed on normal subjects, we had access to a FA due to a special case for one subject where the FA was performed for a different reason. The FA was acquired using a digital fundus camera with a 30° field (Topcon 50 EX; Topcon, Livermore, CA). Sodium fluorescein 25% (2.5 mL) in sterile water (Hub Pharmaceuticals, Rancho Cucamonga, CA) was injected into an antecubital vein using a 25-gauge needle, followed by 5 mL normal saline. Photos were acquired at the time of injection and through the early transit phase in the left eye, followed by photos in the each eye in the mid-transit and late phases. The goal of this comparison was to see that vessels were being properly identified.

We also compared vessels identified using our method under two different laser wavelengths (532 and 840 nm), acquired at different time points, to demonstrate that we could achieve similar results with different imaging sessions and using different imaging parameters.

RESULTS

Video and image processing algorithms were implemented with commercial software (MATLAB; MathWorks, Inc., Natick, MA). The approximate time to construct and analyze a high-quality, eight-video montage of the FAZ using 40-second videos was 2.5 hours, including time for preprocessing and deletion of bad frames. Vessels were mapped for 10 subjects. An example of vessel perfusion mapping is shown for one subject (Fig. 6). For all 10 subjects, FAZs were quantified. The area of the FAZs was 0.323 ± 0.107 mm^2, and the effective diameter was 633 ± 103 μm (mean ± SD), similar to results from other studies (Table).

Since we used some video sets that were acquired for the purpose of other studies, there were some montages that were missing data near the FAZ; thus, we were only able to extract and analyze capillaries on 7 out of the 10 subjects (Fig. 7). The average capillary densities were 34.0, 31.5, 30.3, and 30.7 mm^{-1} in the Superior, Inferior, Nasal, and Temporal (S, I, N, T)
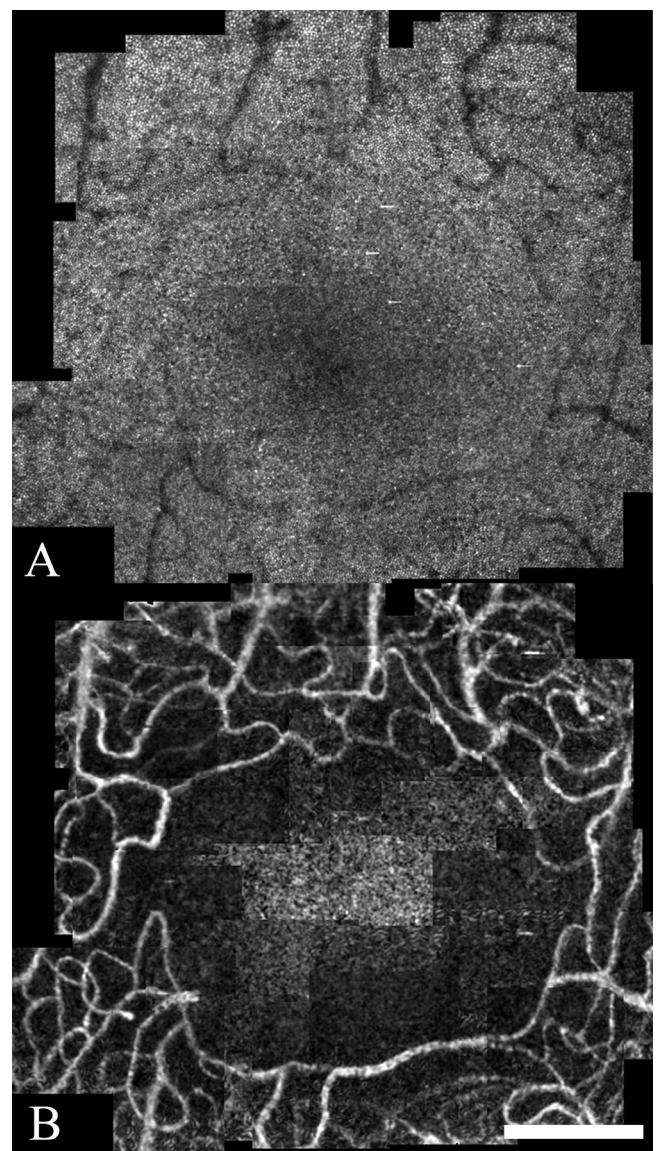
FIGURE 6. Example of capillary mapping in the parafoveal region, using 60 overlapping videos acquired using an 840 nm laser. (A) The montage from unprocessed videos, showing photoreceptors. (B) The montage from processed videos, showing perfused vessels. Scale bar, 300 μm.

TABLE 1. Comparison of FAZ Sizes from Other Studies

Method	Mean Area (mm^2)	Mean Diameter (μm)	Subject Criterion
AOSLO*	0.323	633	No ocular disease
SLO + FA[3]	0.231	542†	Non-diabetics
FA[25]	0.350	730	Non-diabetics
FA[2]	0.221‡	530	10 < Age < 39
	0.292‡	610	Age > 40

　* Our method.
　† Effective diameter calculated from the area.
　‡ Area estimated from diameter measurement.

directions (Fig. 8), similar in magnitude to capillaries in the brain.[16]

　For one subject, the parafoveal region of the FA was extracted and compared with the vessels extracted using our method (Fig. 9). The same eye was imaged twice at different times using different parameters (Fig. 10).

DISCUSSION

This article presents a method to visualize and analyze the FAZ and parafoveal capillary network noninvasively. The approach is based on the idea of using motion as intrinsic contrast. The key assumption is that blood cells move relative to their surrounding photoreceptors; thus, by extracting motion from videos of the eye, one can visualize perfused
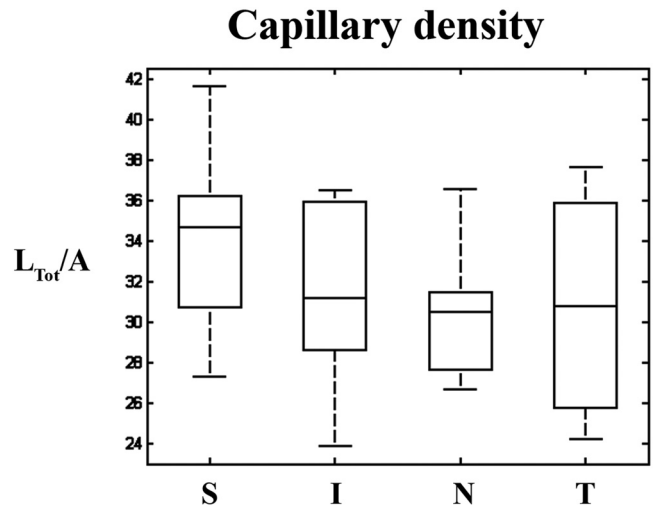

Capillary density

FIGURE 8. Capillary density in four directions (S, I, N, T), where density is defined as L_{Tot}/A, the total length of capillary segments divided by the area of the analysis region. There was no significant difference in densities in four directions ($P = 0.31$).

vessels. Motion is extracted using multi-frame division videos; using division images enables multiple division images to be averaged together arithmetically. This averaging enhances the final SNR. In general, noninvasive videos of the microcirculation from many imaging modalities suffer from
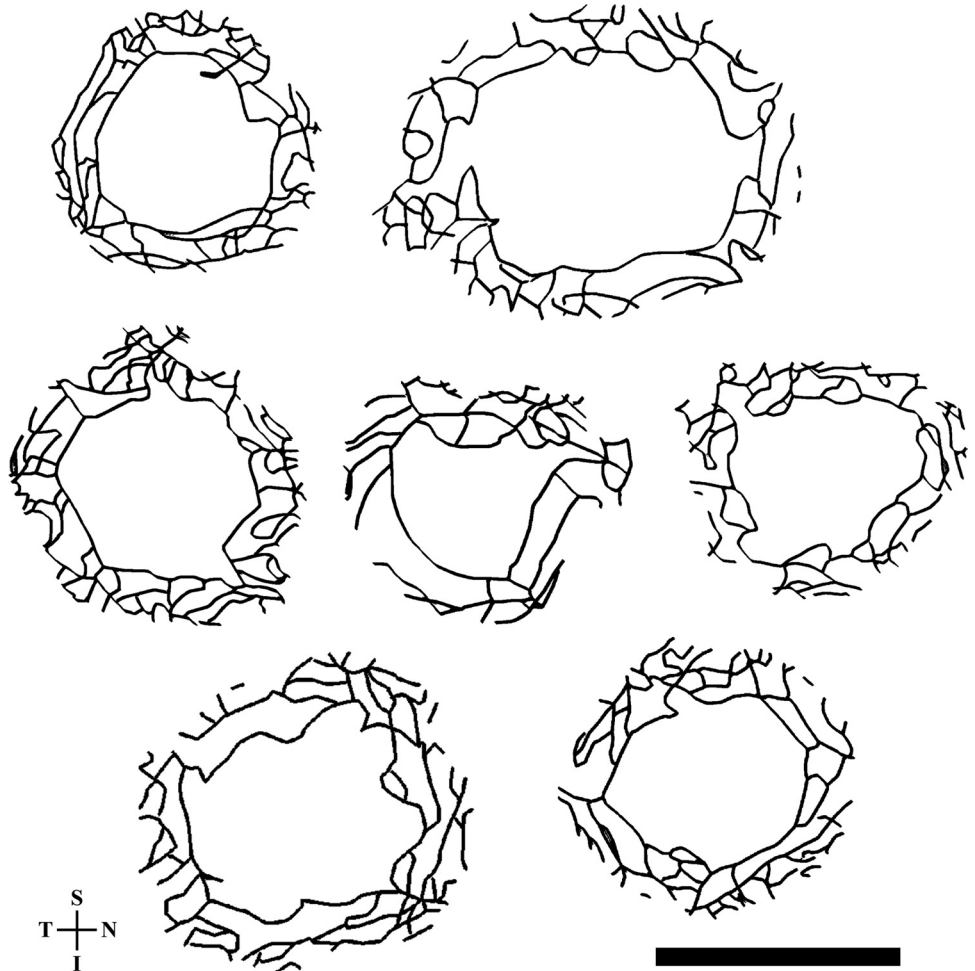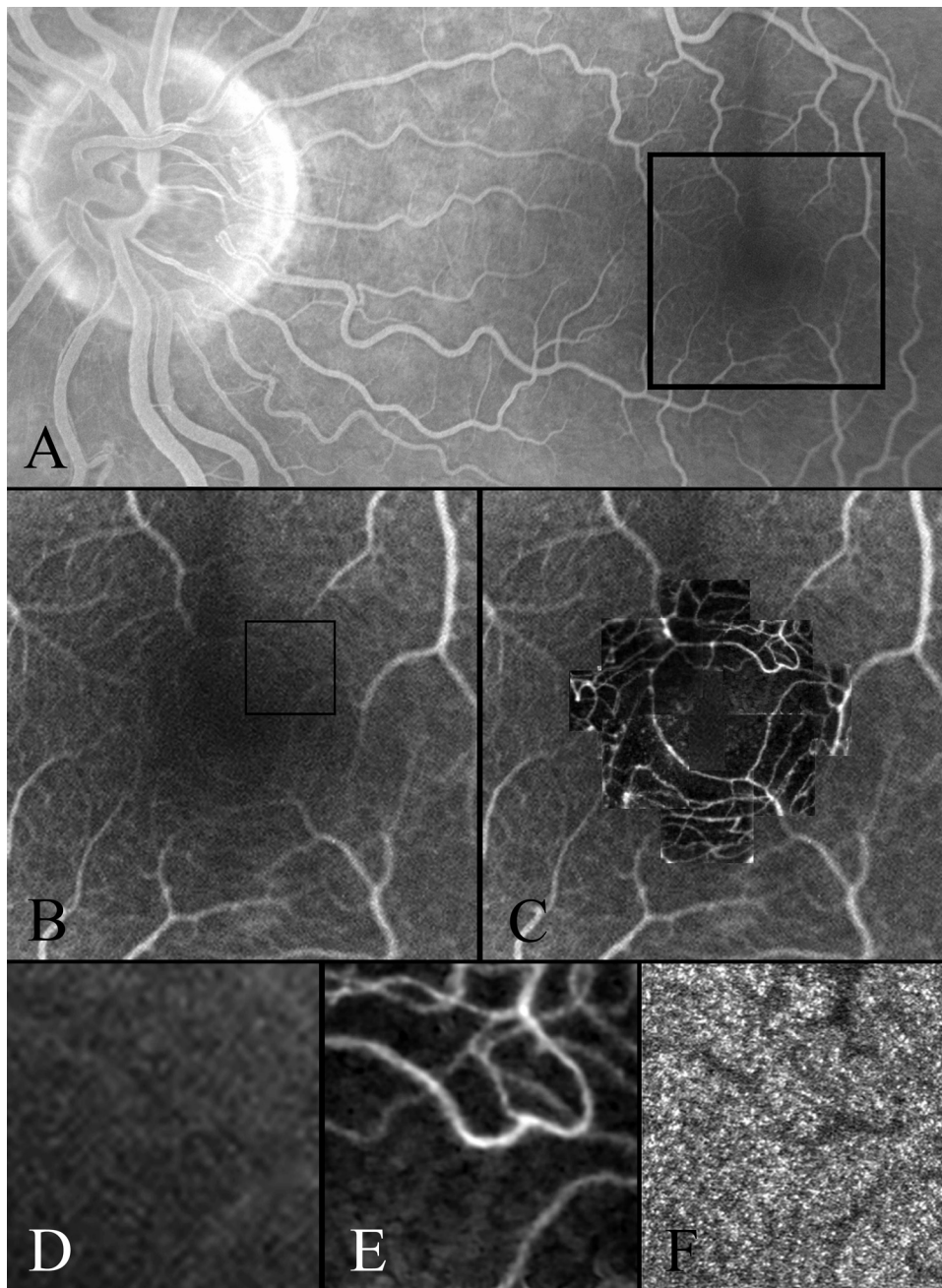

FIGURE 7. Extracted capillaries in the ROI for all the subjects that were analyzed. OD images were flipped horizontally to match OS images, to label the four directions (S, I, N, T). Scale bar, 300 μm.

FIGURE 9. Comparison of FA to our method, for 532 nm videos. (**A**) The posterior pole region from a FA. The *box* shows the location of the fovea and parafoveal capillaries. (**B**) Contrast-enhanced FA in the parafoveal region (*box* from **A**). The location of a single video location is shown in the *small box*. (**C**) Contrast-enhanced FA, with the montage from processed images overlaid. (**D**) Contrast-enhanced FA at the edge of the FAZ (*box* from **B**). (**E**) Image from a single processed video showing perfused capillaries (at *box* from **B**). (**F**) Single frame from the unprocessed video showing photoreceptors (at *box* from **B**).

low contrast, a common challenge for many vessel analysis algorithms. Our technique for motion contrast enhancement is general, and can be applied as an enabling step for more advanced analyses, such as quantification of the FAZ and parafoveal capillary density.

There are several advantages to using this approach. Most importantly, it is noninvasive, and can potentially be applied with low risk for subjects ranging from normal to pre-disease to disease states. The comparison of the vessel montage to FA shows that the method is able to detect retinal capillaries and generate a complete parafoveal map. FAs were not performed on other subjects to avoid unnecessary risks associated for eyes with no ocular conditions. Another advantage of this technique is the availability of other retinal measurements from the same dataset. The photoreceptor mosaic can be analyzed from unprocessed videos (Figs. 6, 9). Also, it is possible to investigate the

speed and pulsatility of individual leukocytes as they move through capillaries, using offline analysis.[10,20] Finally, one can extend the analysis to compute statistics such as vessel density, as illustrated in this article.

The main limitations to the method are: (1) it may be too time consuming for immediate clinical use; (2) subjects must have clear ocular media; and (3) good subject compliance is necessary. First, our technical methods for visualization of the parafoveal capillaries were developed to demonstrate a new concept, and not for immediate clinical implementation. Also, the time to acquire overlapping videos may influence which subjects might be good candidates. Second, there are many potential subjects that have clear ocular media, particularly subjects in normal and pre-diseased states, as well as some subjects with certain diseases; these subjects are usually precluded from invasive procedures such as FA. Finally, while good subject compliance is
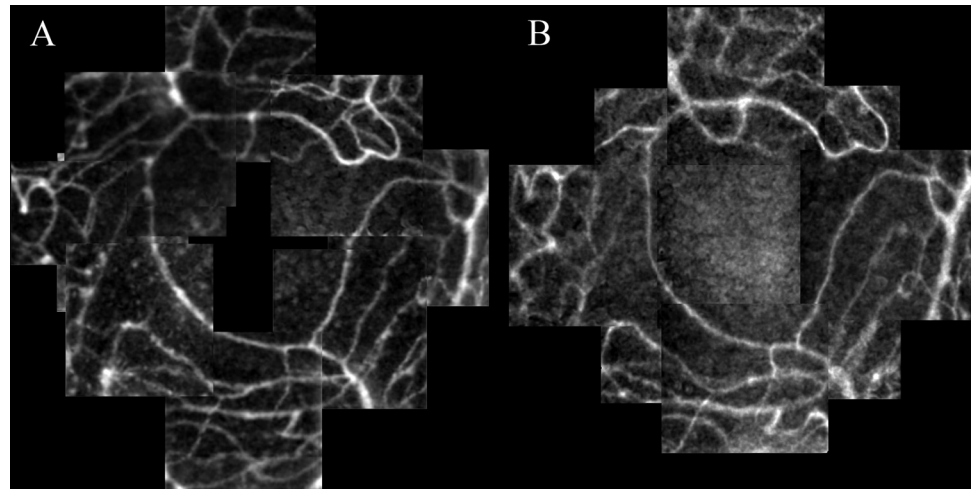
FIGURE 10. Montages of processed videos showing vessels from two separate imaging sessions. The parafoveal region of the same eye was imaged twice: (**A**) using a 532 nm wavelength laser, and (**B**) using an 840 nm wavelength laser, 53 months later.

helpful during imaging sessions, the subject tasks are relatively straightforward, involving fixation on targets presented at various locations.

There are tradeoffs when imaging with two different laser wavelengths. A prior study showed that green laser wavelengths were optimal for vessel contrast in scanning laser ophthalmoscopy (SLO) systems.[21] While we found that the contrast of vessels and flow through vessels was higher for the 532 nm laser compared with the 840 nm laser (Fig. 10), we did not observe any differences in the vessels that could be identified for analysis. However, there are major advantages to using the 840 nm laser. The SNR of the photoreceptors is much higher for videos acquired at 840 nm, an important consideration when evaluating photoreceptor health; this was because we imposed conservative light exposure limits. To ensure safe light levels, the power that reached the subjects' retinas was maintained at a level that was at 10x below the Maximum Permissible Exposure limit defined by the American National Standards Institute.[22] Since the SNR improves as the power of light increases, and since we imposed our conservative light exposure limits, the videos acquired at 532 nm had considerably lower SNRs. Finally, the lower brightness 840 nm light source (~50 trolands) was better for subject comfort.

Despite variations in imaging parameters, we were able to achieve good results overall with our algorithms. Such variation would potentially require variations in video and image processing parameters; however, we were able to apply the same general method to all videos. We also showed that we could achieve similar results using videos from different imaging sessions (Fig. 10). Due to the unique nature of this approach, there are no direct methods to validate the approach other than comparison to FA. Even when contrast agents are combined with SLO,[3,23] the level of detail that we achieved was not observed. Previously, the only established method for noninvasive visualization of the FAZ and parafoveal capillary network was based on the entoptic blue field phenomenon.[24]

There are many areas for future work. Since detection of parafoveal capillaries was the goal of this article, there remains much work in image analysis for automation, enhanced segmentation, classification, and registration of vessels from motion contrast enhanced images. There are also important applications in clinical medicine based on FAZ quantification and capillary density, including the development of potential biomarkers for disease, measures of retinal health in disease progression, or endpoint measures for clinical trials.

References

1. Snodderly DM, Weinhaus RS, Choi JC. Neural-vascular relationships in central retina of macaque monkeys (Macaca fascicularis). *J Neurosci.* 1992;12:1169–1193.
2. Laatikainen L, Larinkari J. Capillary-free area of the fovea with advancing age. *Invest Ophthalmol Vis Sci.* 1977;16:1154–1157.
3. Arend O, Wolf S, Jung F, et al. Retinal microcirculation in patients with diabetes mellitus: dynamic and morphological analysis of perifoveal capillary network. *Br J Ophthalmol.* 1991; 75:514–518.
4. Kwan AS, Barry C, McAllister IL, Constable I. Fluorescein angiography and adverse drug reactions revisited: the Lions Eye experience. *Clin Experiment Ophthalmol.* 2006;34:33–38.
5. Weinhaus RS, Burke JM, Delori FC, Snodderly DM. Comparison of fluorescein angiography with microvascular anatomy of macaque retinas. *Exp Eye Res.* 1995;61:1–16.
6. Japee SA, Ellis CG, Pittman RN. Flow visualization tools for image analysis of capillary network. *Microcirculation.* 2004;11:39–54.
7. Sato Y, Chen J, Zoroofi RA, Harada N, Tamura S, Shiga T. Automatic extraction and measurement of leukocyte motion in microvessels using spatiotemporal image analysis. *IEEE Trans Biomed Eng.* 1997;44:225–236.
8. Liang J, Williams DR, Miller DT. Supernormal vision and high-resolution retinal imaging through adaptive optics. *J Opt Soc Am A.* 1997;14:2884–2892.
9. Roorda A, Romero-Borja F, Donnelly WJ III, Queener H, Hebert TJ, Campbell MCW. Adaptive optics scanning laser ophthalmoscopy. *Opt Express.* 2002;10:405–412.
10. Martin JA, Roorda A. Direct and non-invasive assessment of parafoveal capillary leukocyte velocity. *Ophthalmol.* 2005;12:2219–2224.
11. Arathorn DW, Yang Q, Vogel CR, Zhang Y, Tiruveedhula P, Roorda A. Retinally stabilized cone-targeted stimulus delivery. *Opt Express.* 2007;15:13731–13744.
12. Vogel CR, Arathorn DW, Roorda A, Parker A. Retinal motion estimation in adaptive optics scanning laser ophthalmoscopy. *Opt Express.* 2006;14:487–497.
13. Frangi AF, Niessen WJ, Vincken KL, Viergever MA. Multiscale vessel enhancement filtering. *Med Image Comput Comput Assist Interv.* 1998:130–137.
14. Bennett AG. *Clinical Visual Optics.* 2nd ed. Oxford: Butterworth-Heinemann; 1990.

15. Bennett AG, Rudnicka AR, Edgar DF. Improvements on Littmann's method of determining the size of retinal features by fundus photography. *Graefe's Arch Clin Exp Ophthalmol.* 1994;232:361–367.

16. Zheng D, LaMantia A-S, Purves D. Specialized vascularization of the primate visual cortex. *J Neurosci.* 1991;11:2622–2629.

17. Blum H. A transformation for extraction new descriptors of shape. In: Wathen-Dunn W, ed. *Models for the Perception of Speech and Visual Form.* Cambridge, MA: MIT Press; 1967:362–380.

18. Michaelson IC. *Retinal Circulation in Man and Animals.* Springfield, IL: Charles C Thomas; 1954.

19. Glantz SA. *Primer of Biostatistics.* 5th ed. New York: McGraw Hill; 2002.

20. Martin JA, Roorda A. Pulsatility of parafoveal capillary leukocytes. *Exp Eye Res.* 2009;88:356–360.

21. Reinholz F, Ashman RA, Eikelboom RH. Simultaneous three wavelength imaging with a scanning laser ophthalmoscope. *Cytometry.* 1999;37:165–170.

22. American National Standard for the Safe Use of Lasers. ANSI Z136.1–2007. New York: American National Standard Institute; 2007.

23. Paques M, Boval B, Richard S, et al. Evaluation of fluorescein-labeled autologous leukocytes for examination of retinal circulation in humans. *Curr Eye Res.* 2000;37:165–170.

24. Bradley A, Zhang H, Applegate RA, Thibos LN, Elsner AE. Entoptic image quality of the retinal vasculature. *Vision Res.* 1998;38:2685–2696.

25. Bresnick GH, Condit R, Syrjala S, Palta M, Groo A, Korth K. Abnormalities of the foveal avascular zone in diabetic retinopathy. *Arch Ophthalmol.* 1984;102:1286–1293.